We are IntechOpen, the world's leading publisher of Open Access books Built by scientists, for scientists

6,900
Open access books available

186,000
International authors and editors

200M
Downloads

Our authors are among the

154
Countries delivered to

TOP 1%
most cited scientists

12.2%
Contributors from top 500 universities

CLARIVATE ANALYTICS
BOOK CITATION INDEX
INDEXED

WEB OF SCIENCE™

Selection of our books indexed in the Book Citation Index
in Web of Science™ Core Collection (BKCI)

Interested in publishing with us?
Contact book.department@intechopen.com

Numbers displayed above are based on latest data collected.
For more information visit www.intechopen.com

Photonic Crystal Fiber for Medical Applications

Feroza Begum and Yoshinori Namihira
*Graduate School of Engineering and Science, University of the Ryukyus, Okinawa,
Japan*

1. Introduction

Optical coherence tomography (OCT) is a new technology for noninvasive cross-sectional imaging of tissue structure in biological system by directing a focused beam of light at the tissue to be image [Bouma et al., 1995; Jiang et al., 2005; Ryu et al., 2005]. The technique measures the optical pulse time delay and intensity of backscattered light using interferometry with broadband light sources or with frequency swept lasers. It is analogous to ultrasound imaging or radar, except that it uses light rather than sound or radio waves. In addition, unlike ultrasound, OCT does not require direct contact with the tissue being imaged. OCT depends on optical ranging; in other words, distances are measured by shining a beam of light onto the object, then recording the optical pulse time delay of light. Since the velocity of light is so high, it is not possible to directly measure the optical pulse time delay of reflections; therefore, a technique known as low-coherence interferometry compares reflected light from the biological tissue to that reflected from a reference path of known length. Different internal structures produce different time delays, and cross-sectional images of the structures can be generated by scanning the incident optical beam. Earlier OCT systems typically required many seconds or minutes to generate a single OCT image of tissue structure, raising the likelihood of suffering from motion artifacts and patient discomfort during *in vivo* imaging. To counter such problems, techniques have been developed for scanning the reference arm mirror at sufficiently high speeds to enable real-time OCT imaging [Tearnery et al., 1997]. OCT can be used where excisional biopsy would be hazardous or impossible, such as imaging the retina, coronary arteries or nervous tissue. OCT has had the largest impact in ophthalmology where it can be used to create cross-sectional images of retinal pathology with higher resolution than any other noninvasive imaging technique. Now a days OCT is a prospective technology which is used not only for ophthalmology but also for dermatology, dental as well as for the early detection of cancer in digestive organs. The wavelength range of the OCT light source is spread from the 0.8 to 1.6 µm band. This spectral region is of particular interest for OCT because it penetrates deeply into biological tissue and permits spectrally resolved imaging of water absorption bands. In this spectral region, attenuation is minimum due to absorption and scattering. It should be noted that scattering decreases at longer wavelengths in proportion to $1/\lambda^4$, indicating that the scattering magnitude at 0.8 ~ 1.6 µm wavelengths is lower than at the visible wavelengths [Agrawal, 1995]. Ultrahigh-resolution OCT imaging in the spectral region from 0.8 to 1.6 µm requires extremely broad bandwidths because longitudinal resolution depends on the coherence length. The coherence length is inversely proportional to the bandwidth and proportional to square of the light source center wavelength. This can

be achieved by supercontinuum (SC) light using photonic crystal fibers. The ophthalmology and dermatology OCT imaging are done predominantly at near 0.8 μm center wavelength [Bouma et al., 1995; Drexler et al., 1999; Ohmi et al., 2004; Pan et al., 1998; Welzel et al., 1997]. The dentistry OCT imaging is performed at 1.3 μm wavelength [Boppart et al., 1998; Colston et al., 1998; Hartl et al., 2001; Herz et al., 2004]. Currently, it is reported that the OCT imaging at 1.5 ~ 1.6 μm broadband light source can be readily applied to take images of human tooth samples [Lee et al., 2009]. On the other hand, telecommunication window (around 1.55 μm) is the most attractive window in optical communication systems, dispersion compensation and nonlinear optics because of the minimum transmission loss of the fiber [Begum et al., 2007a, 2007b, 2009a].

Photonic crystal fibers (PCFs) [Russel, 2003], a pure silica core optical fibers with tiny air holes embedded in the host silica matrix running along the propagation axis, have boosted the fiber optic research due to their remarkable modal properties such as provide single-mode operation for very short operating wavelengths [Knight et al., 1996], remain single-mode for large scale fibers [Knight et al., 1998], achieve high birefringence [Kaijage et al., 2000], and controllable dispersion characteristics [Begum et al., 2009b] which cannot be achieved with conventional optical fibers. These fibers are also termed as microstructured fibers (MSFs) or microstructured optical fibers (MOFs). PCFs are dived into two categories according to the light confinement mechanisms: one is index-guiding or solid core fibers [Knight et al., 1996] and the other is photonic bandgap (PBG) or hollow core fibers [Couny et al., 2008]. Those with a solid core light can confine in a high-index core by modified total internal reflection which is same index guiding principle as conventional optical fibers. However, they can have a much higher effective-index contrast between core and cladding, and therefore can have much stronger confinement for applications in nonlinear optical devices, polarization maintaining fibers, etc. Alternatively, in PBG fibers where the light is confined in a lower index core by a photonic bandgap created by the microstructured cladding. The presence of air holes in the cladding gives rise to strong wavelength dependence of the cladding index which is primarily responsible for its magnificent characteristics. The extra degrees of freedom in PCFs facilitate a complete control on its properties such as ultraflattened dispersion and high negative dispersion. The precise control of geometrical parameters can provide ultraflattened dispersion in PCFs. PCFs are very attractive and efficient to produce high power light source in OCT system. Because PCFs can generate SC spectrum due to their design degree of freedom which make it possible to enhance the nonlinear effects by reducing effective area and tailor chromatic dispersion. As it is well known, the optical attenuation sources in PCFs include intrinsic losses due to Rayleigh scattering, imperfection losses due to the fabrication, and confinement losses caused by finite number of air holes in the cladding. Since the core has the same refractive index as the cladding, the guided mode is intrinsically leaky and experiences confinement losses. In fact, confinement losses occur even in the absence of the other two losses. By careful design, it is possible to reduce confinement losses to negligible values compared with the intrinsic losses. Control of chromatic dispersion keeping a low confinement loss to a level below the Rayleigh scattering limit is a very important for any optical system supporting ultrashort soliton pulse propagation [Agrawal, 1995]. In all cases, almost flattened fiber dispersion and low confinement loss behavior becomes a crucial issue. Although the resolution power of the currently available OCT machines are remarkable, they are not sufficiently high to unequivocally identify all retinal sublayers and make 'biopsy'-like diagnoses. Resolution is limited mainly by the bandwidth of the light source,

usually a superluminescent diode (SLD) [Colston et al., 1998; Ryu et al., 2005] and increased resolution will require wider bandwidth light sources. The emergence of ultrabroad bandwidth femtosecond laser technology has allowed the development of an ultra-high resolution OCT [Boppart et al., 1998; Bouma et al., 1995; Drexler et al., 1999; Hartl et al., 2001; Herz et al., 2004; Jiang et al., 2005; Lee et al., 2009; Ohmi et al., 2004; Pan et al., 1998; Tearnery et al., 1997; Welzel et al., 1997]. The ultrahigh resolution OCT will in effect be a microscope capable of revealing certain histopathological aspects of macular disease in the living tissue. Femtosecond laser source is expensive than picosecond laser source and low incident power. Consequently, currently researchers are paying attention to develop picosecond light sources for using ultrahigh-resolution OCT system. Picosecond pulse laser source gives more narrow spectra than femtosecond laser source but since the laser source is cheaper in this case it attracts practical implementation. The ultrahigh resolution OCT will in effect be a microscope capable of revealing certain histopathological aspects of macular disease in the living tissue.

In this work, we report a broadband SC generation in highly nonlinear photonic crystal fiber (HN-PCF) at center wavelength 0.8 μm, 1.3 μm and 1.55 μm using high power picosecond pulses which can be applicable in ultrahigh-resolution OCT system for ophthalmology, dermatology and dental imaging. The proposed HN-PCF is investigated through a full-vector finite difference method with anisotropic perfectly matched layer. Through numerical simulation, it is demonstrated that it is possible to achieve different properties of the proposed HN-PCF. Based on the nonlinear Schrödinger equation, we find that the proposed HN-PCF, having four rings and two different sizes of air holes, can achieve SC spectrum with input picosecond pulses. We have further investigated the full width of half maximum of the generated SC spectrum of HN-PCF that can gives significant information on the longitudinal resolution in biological tissue by assuming coherent length. The achieved longitudinal resolutions in tissue are 0.97 μm at 0.8 μm for ophthalmology and dermatology, 0.85 μm at 1.3 μm for dental imaging and 1.1 μm at 1.55 μm also for dental imaging. To our knowledge, these are the highest resolution achieved in biological tissue to date at 0.8 μm, 1.3 μm and 1.55 μm wavelength. Furthermore, numerical simulation result shown that it is possible to obtain ultra-flattened chromatic dispersion, low dispersion slope, high nonlinear coefficient and very low confinement loss, simultaneously from the proposed HN-PCF.

2. Proposed HN-PCF structure

Fig. 1 (a) shows the schematic cross section of the conventional PCF structure. This PCF consists of a triangular lattice of air holes where the core is defined by a missing air hole. The core diameter is 2a, where 'a' equals Λ-d/2. The air hole pitch is labeled Λ, and measures the period of the air hole structure (the distance between the centers of neighboring air holes). The air hole size is labeled d, and measures the diameter of the holes. The background material is regular silica with a cladding refractive index n = 1.45. Fig. 1 (b) shows the proposed HN-PCF structure. It has a pitch Λ, two air holes with diameters d_1 and d. The pitch constant is chosen to be Λ = 0.87 μm, while the diameter of the air holes in the cladding of the fiber are d_1 = 0.46 μm, d = 0.80 μm, with a total number of 4 hole layers in the cladding. Designing HN-PCF for the OCT and telecommunication window using a conventional PCF structure is difficult: therefore, the dimensions of the first rings of the proposed HN-PCF are scaled downed to shape the dispersion characteristics. The dimensions of the other rings are retained sufficiently large for better field confinement.
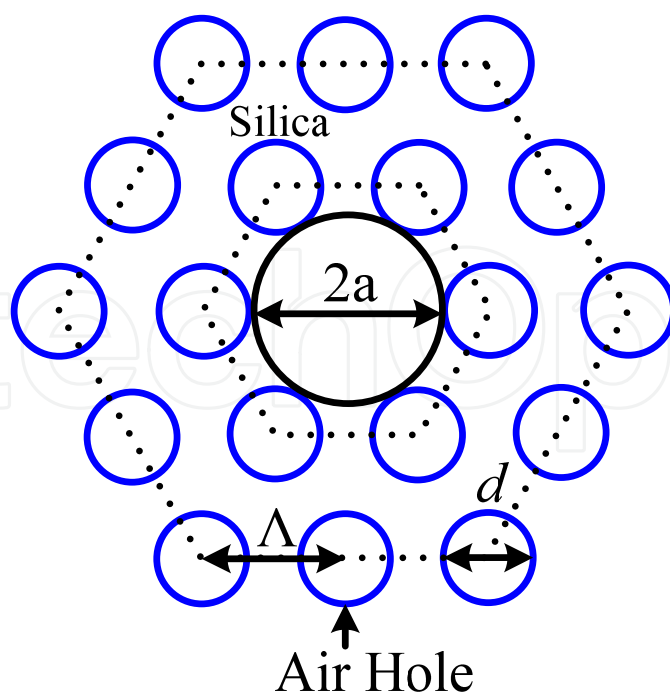
Fig. 1(a). Schematic cross section of the conventional PCF structure.
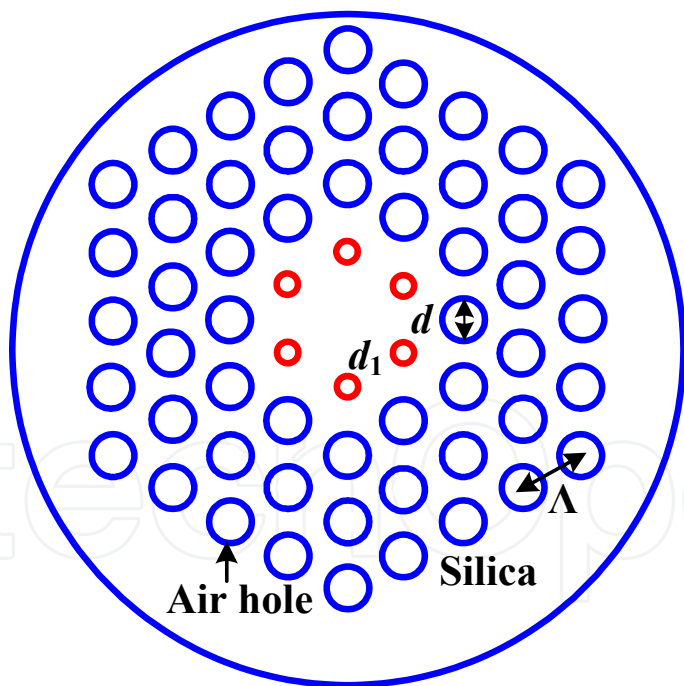

Fig. 1(b). The proposed HN-PCF structure.

This HN-PCF structure can provide ultra-flattened chromatic dispersion characteristics with very high nonlinearity, and low confinement loss for the OCT and telecommunication window. We analyzed the proposed HN-PCF with low confinement losses by modulating only dimension of the first rings, in order to simplify the structure and decrease the fabrication difficulties. In telecommunication widow, the parameters Λ = 0.79 μm, d_1 = 0.28

µm, d = 0.69 µm, with a total number of 7 hole layers in the cladding are selected for achieving ultra-flattened chromatic dispersion characteristics, small effective area, and low confinement loss. In this case, 7 air hole layers are selected only for reducing confinement loss below 0.2 dB/km.

3. Numerical model

The situation in photonics is especially favorable for computation because the Maxwell equations are practically exact, the relevant material properties are well known, and the length scales are not too small. The results of such computations have consistently agreed with experiments. This makes it possible and preferable to optimize the design of photonic crystals on a computer, and then manufacture them. For this proposed HN-PCF structure, by using an accurate modal analysis based on a full-vector finite difference method (FDM) [Begum et al., 2011; Shen et al., 2003] with anisotropic perfectly matched boundary layers (PML), we evaluate the different properties of HN-PCF. The PML in fact is not a boundary condition, but an additional domain that absorbs the incident radiation waves without producing reflections. Once the effective refractive index n_{eff} is obtained by solving an eigenvalue problem drawn from the Maxwell's equations using the FDM, the parameter chromatic dispersion $D(\lambda)$, confinement loss L_c, effective area A_{eff} and nonlinear coefficient γ can be calculated [Begum et al., 2011; Shen et al., 2003].

3.1 Chromatic dispersion

The group-velocity dispersion $D(\lambda)$ is defined as the change in pulse width per unit distance of propagation (i.e., ps/(nm.km). It means that $D(\lambda)$ causes a short pulse of light to spread in time as a result of different frequency components of the pulse traveling at different velocities. This can be calculated from following equation.

$$D(\lambda) = \frac{d\beta_1}{d\lambda} = \frac{d}{d\lambda}\left(\frac{1}{v_g(\lambda)}\right) = -\frac{2\pi c}{\lambda^2}\beta_2 = -\frac{\lambda}{c}\frac{d^2 \operatorname{Re}[n_{eff}]}{d\lambda^2} \tag{1}$$

where, β_1 and β_2 are the propagation constant parameters, v_g is the group velocity, λ is the operating wavelength in µm, c is the velocity of the light in a vacuum, $\operatorname{Re}[n_{eff}]$ is the real part of the effective index.
The corresponding dispersion slope $S(\lambda)$ is defined as

$$S(\lambda) = \frac{dD(\lambda)}{d\lambda} \tag{2}$$

Since the total chromatic dispersion is the summation of material dispersion $D_m(\lambda)$ and waveguide dispersion $D_w(\lambda)$. The material dispersion quantified from the Sellmeier equation is directly included in the FDM calculation process. The reason for this is that $D_m(\lambda)$ is mostly determined by the wavelength dependence of the fiber material and for this reason it cannot be altered significantly in the engineering process. On the other hand, $D_w(\lambda)$, which is strongly dependent to the silica-air structure. Therefore, in our calculation chromatic dispersion $D(\lambda)$ [Begum et al., 2011; Shen et al., 2003] corresponds to the total dispersion of the PCFs.

3.2 Confinement loss

The attenuation caused by the waveguide geometry is called confinement loss L_c. This is an additional form of loss that occurs in single-material fibers particularly in PCFs because they are usually made of pure silica and given by [Begum et al., 2011; Shen et al., 2003]

$$L_c = -20\log_{10} e^{-k_0 \text{Im}[n_{eff}]} = 8.686 k_0 \text{Im}[n_{eff}]$$

(3)

where, k_0 is the propagation constant in free space, λ is the operating wavelength in μm, and Im(n_{eff}) is the imaginary part of the complex effective index n_{eff}.

3.3 Effective area

The effective area A_{eff} is defined as follows [Begum et al., 2011; Shen et al., 2003]

$$A_{eff} = \frac{(\int\limits_{-\infty}^{\infty} \int\limits_{-\infty}^{\infty} |E|^2 \ dxdy)^2}{\int\limits_{-\infty}^{\infty} \int\limits_{-\infty}^{\infty} |E|^4 \ dxdy}$$

(4)

where, E is the electric field derived by solving Maxwell's equations. From this equation, it is seen that effective area A_{eff} depends on the fiber parameters such as the mode field diameter and core-cladding index difference.

3.4 Nonlinear coefficient

In this research, silica is used as a background material for designing PCFs. Since silica can be treated as a homogeneous material, the lowest-order nonlinear coefficient is the third-order susceptibility $\chi^{(3)}$. Most of the nonlinear effects in optical fibers therefore originate from nonlinear refraction, a phenomenon that refers to the intensity dependence of the refractive index resulting from the contribution of $\chi^{(3)}$, i.e., the refractive index of the fiber becomes [Agrawal, 1995]

$$n = n_1 + n_2 E^2$$

(5)

where, n_1 is the linear refractive index which is responsible for material dispersion, E^2 is the optical intensity inside the fiber, n_2 is the nonlinear refractive index related to $\chi^{(3)}$ by the following relation

$$n_2 = \frac{3}{8n_1} \text{Re}\left(\chi^{(3)}_{\chi\chi\chi\chi}\right)$$

(6)

where, Re stands for the real part. Another way to represents the refractive index is

$$n = n_1 + n_2 \frac{P}{A_{eff}}$$

(7)

where, P is the incident light power and A_{eff} is the effective area of the fiber. From nonlinear part of Eq. (5) and Eq. (7), we can write

$$E^2 = \frac{P}{A_{eff}} \tag{8}$$

From Eq. (8), it is clear that optical intensity inside the fiber E can be increased by two ways. One is by focusing the light tightly to reduced A_{eff} and by increasing incident optical power. The nonlinear coefficient of PCFs depends on the value of nonlinear refractive index and the effective area of the PCFs. The nonlinear coefficient is calculated according to following equation [Agrawal, 1995].

$$\gamma = \left(\frac{\omega}{c}\right)\left(\frac{n_2}{A_{eff}}\right) = \left(\frac{2\pi}{\lambda}\right)\left(\frac{n_2}{A_{eff}}\right) \tag{9}$$

where, γ is the nonlinear coefficient, ω is the angular frequency, n_2 is the nonlinear refractive index, λ is the wavelength of the light, (n_2/A_{eff}) is the nonlinear constant. It is possible to enhance the nonlinearity by reducing the effective area A_{eff} through a smaller core diameter and increasing nonlinear refractive index of a material n_2. This n_2 is constant and depending on the material of the fibers while is variable and varied from $2.2 \sim 3.4 \times 10^{-20}$ m^2/W.

3.5 Nonlinear Schrödinger equation

Nonlinear Schrödinger equation (NLSE) is used for numerical calculation of SC spectrum [Agrawal, 1995]. The propagation equation Eq. (10) is a nonlinear partial differential equation that does not generally lend itself to analytic solutions when both the nonlinearity and the dispersion effect are present. A numerical approach is therefore often necessary for an understanding of the nonlinear effects in optical fibers. The split-step Fourier method is one of these, and is the most popular algorithm because of its good accuracy and relatively modest computing time [Agrawal, 1995].

$$\frac{\partial A}{\partial Z} + \frac{\alpha}{2}A + \frac{i}{2}\beta_2\frac{\partial^2 A}{\partial T^2} - \frac{1}{6}\beta_3\frac{\partial^3 A}{\partial T^3} = i\gamma\left[|A|^2 A + i\frac{\lambda_c}{2\pi c}\frac{\partial}{\partial T}\left(|A|^2 A\right) - T_R A\frac{\partial |A|^2}{\partial T}\right] \tag{10}$$

where, A is the complex amplitude of the optical field, z is the propagation distance, a is the attenuation constant of the fiber, $T = t - z/v_g$ (t is the physical time, v_g is the group velocity at the center wavelength), γ is the nonlinear coefficient, λ_c is the center wavelength, and T_R is the slope of the Raman gain, β_n (n =1 to 3) are the n-th order propagation constant. This propagation constant $\beta(\omega)$ is approximated by a few first terms of a Taylor series expansion about the carrier frequency ω_0, that is

$$\beta(\omega) = \beta_0 + (\omega - \omega_0)\beta_1 + \frac{1}{2}(\omega - \omega_0)^2\beta_2 + \frac{1}{6}(\omega - \omega_0)^3\beta_3 + \cdots \tag{11}$$

where,

$$\beta_n = \left(\frac{d^n\beta}{d\omega^n}\right)_{\omega = \omega_0} \tag{12}$$

The second order propagation constant β_2 [ps^2/km], accounts for the dispersion effects in fiber-optic communication systems. Depending on the sign of β_2, the dispersion region can

be classified into two regions, normal dispersion region ($\beta_2 > 0$) and anomalous dispersion region ($\beta_2 < 0$).

3.6 Coherence length

Coherence length l_c is one of the important parameter in estimating the longitudinal resolution of the OCT source. The shorter the coherence length of the source, the more closely the sample and reference arm group delays must be matched for the constructive interference to occur. On the other word, we can say the combination of the reflected light from the sample arm (containing the item of the interest) and the reference light from the reference arm (usually a mirror) gives rise to an interference pattern but only if light from both arms traveled the same optical distance. The same optical distance means a difference of less than a coherence length. For a Gaussian spectrum the FWHM-duration of the coherence time t_c is

$$t_c = \frac{4\ln 2}{\pi \Delta v} \tag{13}$$

where, the half-power bandwidth Δv represents the spectral bandwidth of the source in the optical frequency domain.

Because of the backscattering configuration of OCT that the light travels back and forth in the interferometer, the coherence length l_c (in air) is expressed by the formula [Bouma et al., 1995]

$$l_c = \frac{ct_c}{2} = \frac{2c\ln(2)}{\pi} \cdot \frac{1}{\Delta v} = \frac{2\ln(2)}{\pi} \cdot \frac{\lambda_c^2}{\Delta \lambda} \tag{14}$$

$$l_c \approx 0.44 \frac{\lambda_c^2}{\Delta \lambda} \tag{15}$$

where, c is the velocity of light in free-space, λ_c is the center wavelength of the spectrum and $\Delta\lambda$ is the FWHM-wavelength width, $\Delta v = \frac{c\Delta\lambda}{\lambda_c^2}$ is the spectral bandwidth. This l_c is very important for estimating the longitudinal resolution l_r in air and biological tissue.

3.7 Longitudinal resolution

The axial or longitudinal and lateral or transverse resolutions of OCT are decoupled from one another; the former being an equivalent to the coherence length l_c of the light source and the latter being a function of the optics. After calculating coherence length l_c, longitudinal resolution in air and biological tissue can be estimated by [Bouma et al., 1995]

$$l_r = \frac{l_c}{n_{tissue}} \tag{16}$$

where, n_{tissue} is the refractive index of the biological tissue. For ultrahigh-resolution OCT imaging l_c should be low value because l_r is proportional with l_c.

4. Simulation results

Fig. 2 (a), (b) and (c) shows the wavelength dependence properties of chromatic dispersion, dispersion slope, effective area, nonlinear coefficient and confinement loss for the four-rings

HN-PCF in Fig. 1. As shown in Fig. 1, only the diameter of the first air hole ring is varied and the diameters of the remaining air holes remain the same, where d_1 = 0.46 µm, d = 0.80 µm, for a fixed pitch Λ = 0.87 µm. From Fig. 2, it is found that the proposed HN-PCF owning ultra-flattened chromatic dispersion and dispersion slope at 0.8 µm are 0.55 ps/(nm.km) and 0.2 ps/(nm^2.km), respectively. The nonlinear coefficient is larger than 208.0 [W·km]$^{-1}$ at 0.8 µm wavelength. Besides, the confinement loss is calculated and it is found that confinement loss is less than 10^{-2} dB/km in the wavelength range of 0.75 µm to 1.0 µm which is lower than Rayleigh scattering loss in conventional fiber.

Fig. 3 (a), (b) and (c) demonstrates the wavelength dependence properties of chromatic dispersion, confinement loss and effective area for the seven-rings HN-PCF in Fig. 1, where d_1 = 0.28 µm, d = 0.69 µm, for a fixed pitch Λ = 0.79 µm. In this case, it has been selected 7 air hole rings for reducing confinement loss lower than Rayleigh scattering loss in conventional fiber at 1.55 µm. Numerical simulation results show that the 7-rings HN-PCF have nonlinear coefficients more than 54.0 [W·km]$^{-1}$ and confinement loss lower than 0.1 dB/km at 1.55 µm, ultra-flattened chromatic dispersion of -2.3 ps/(nm.km) at 1.55 µm wavelength.

SC generation in the proposed HN-PCF is numerically calculated which is shown in Fig. 4 (a), (b) and (c). In Fig. 4 consider the propagation of the sech^2 (square of the hyperbolic-secant) waveform with the full width at half maximum (FWHM), T_{FWHM} and Raman scattering parameter are 1.0 ps and 3.0 fs, respectively, through the proposed HN-PCF. The input power P_{in} of the incident pulses are 18.0 W, 55.0 W and 58.0 W at 0.8 µm, 1.3 µm and 1.55 µm, respectively. The propagation constant around the carrier frequency β_2 and β_3 are 1.88 ps^2/km and 0.02 ps^3/km, respectively for Fig. 4 (a). Again, the propagation constant around the carrier frequency β_2 and β_3 are 2.55 ps^2/km and -0.03 ps^3/km, respectively for Fig. 4 (b). Moreover, the propagation constant around the carrier frequency β_2 and β_3 are 1.51 ps^2/km and 0.01 ps^3/km, respectively for Fig. 4 (c). The achieved fiber length is 10.0 m in all cases. The calculated SC spectrum FWHM bandwidth is 200 nm, 530 nm and 590 nm at center wavelength 0.8 µm, 1.3 µm and 1.55 µm, respectively. From these results, it is evident that high quality SC spectrum is readily generated with relatively short fiber length and good incident power compared to the previously reported ones [Boppart et al., 1998; Bouma et al., 1995; Colston et al., 1998; Drexler et al., 1999; Hartl et al., 2001; Herz et al., 2004; Jiang et al., 2005; Lee et al., 2009; Ohmi et al., 2004; Pan et al., 1998; Ryu et al., 2005; Tearnery et al., 1997; Welzel et al., 1997].

Fig. 5 (a), (b) and (c) represents the intensity spectra of the proposed HN-PCF at center wavelengths 0.8 µm, 1.3 µm and 1.55 µm, respectively when changing incident optical powers. It should be noted that in this time, the fiber lengths are remain unchanged in all of the center wavelengths. From these figures, it is seen that intensity spectra are gradually broadening with increasing the input power, P_{in} at the particular wavelength. Therefore, it is clearly seen that the SC spectral width is dependent to the incident power.

Fig. 6 (a), (b) and (c) represents the intensity spectra of the proposed HN-PCF at center wavelengths 0.8 µm, 1.3 µm and 1.55 µm, respectively in different fiber lengths while incident optical powers are remain unchanged. From these figures, it is observed that intensity spectra are gradually broadening with increasing the fiber length, L_F at the particular wavelength. So, it is noted that the SC spectral width is dependent to the fiber length. From Fig. 5 and 6, it is clear that the SC spectral width is dependent to the incident power and fiber length as well.

Fig. 7 (a), (b) and (c) demonstrates the output powers of the proposed HN-PCF at center wavelengths 0.8 µm, 1.3 µm and 1.55 µm, respectively when the fiber length is 10 m in all center wavelengths. From these figures, it is found that output powers are increased with increasing incident input powers at particular wavelength.
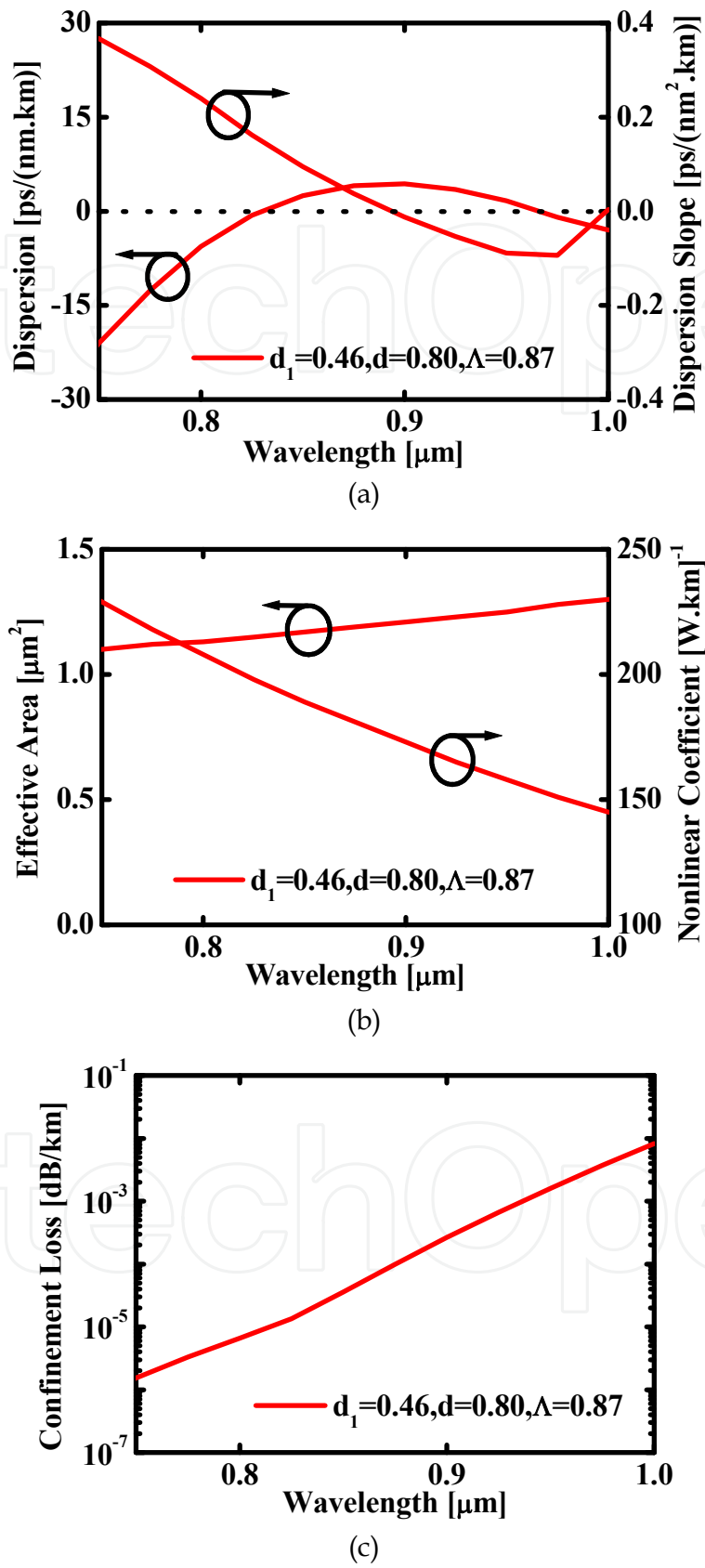
(a)

(b)

(c)

Fig. 2. (a) Chromatic dispersion and dispersion slope, (b) Effective area and nonlinear coefficient and (c) Confinement loss of the 4-rings proposed HN-PCF.
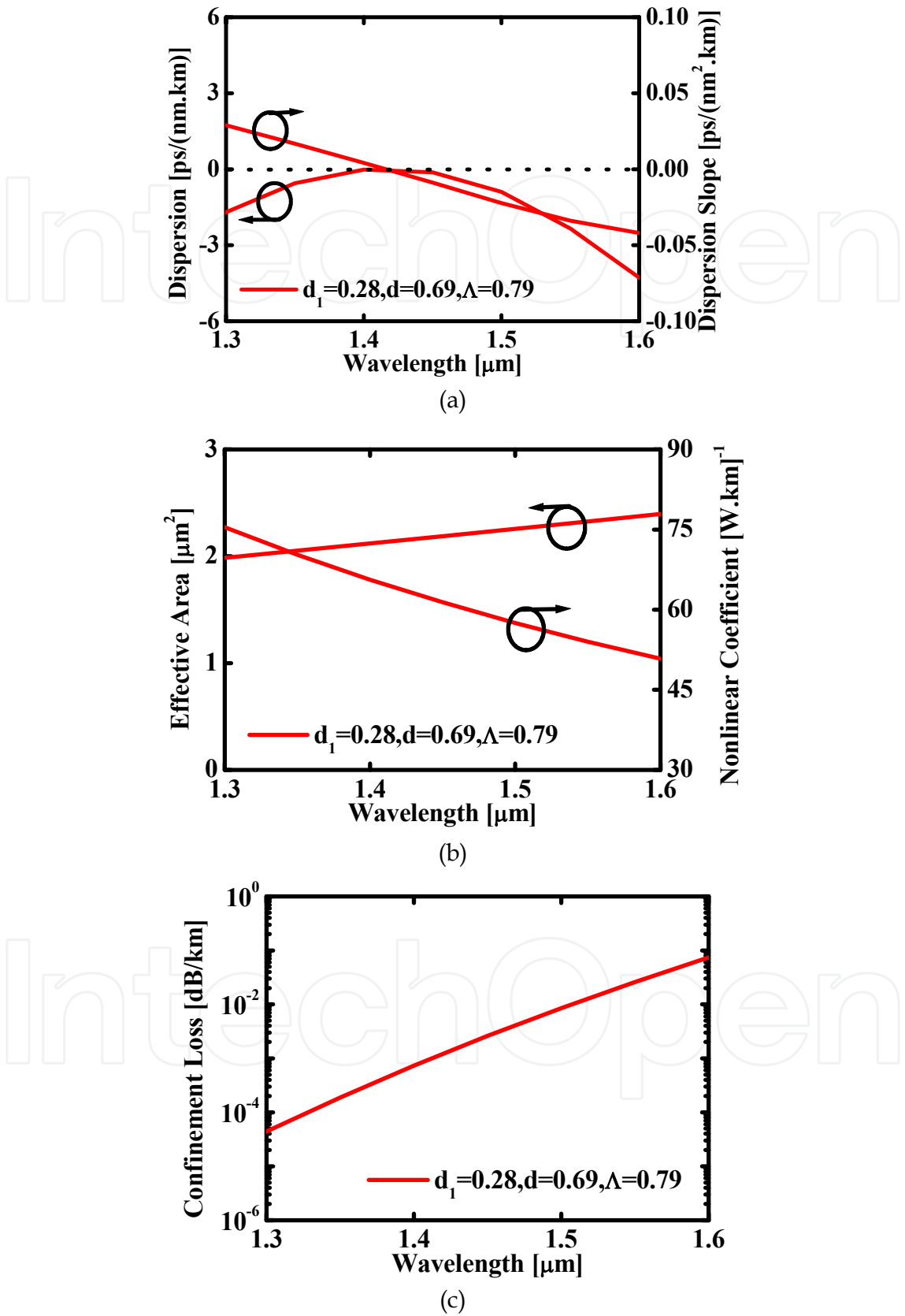
Fig. 3. (a) Chromatic dispersion and dispersion slope, (b) Effective area and nonlinear coefficient and (c) Confinement loss of the 7-rings HN-PCF.
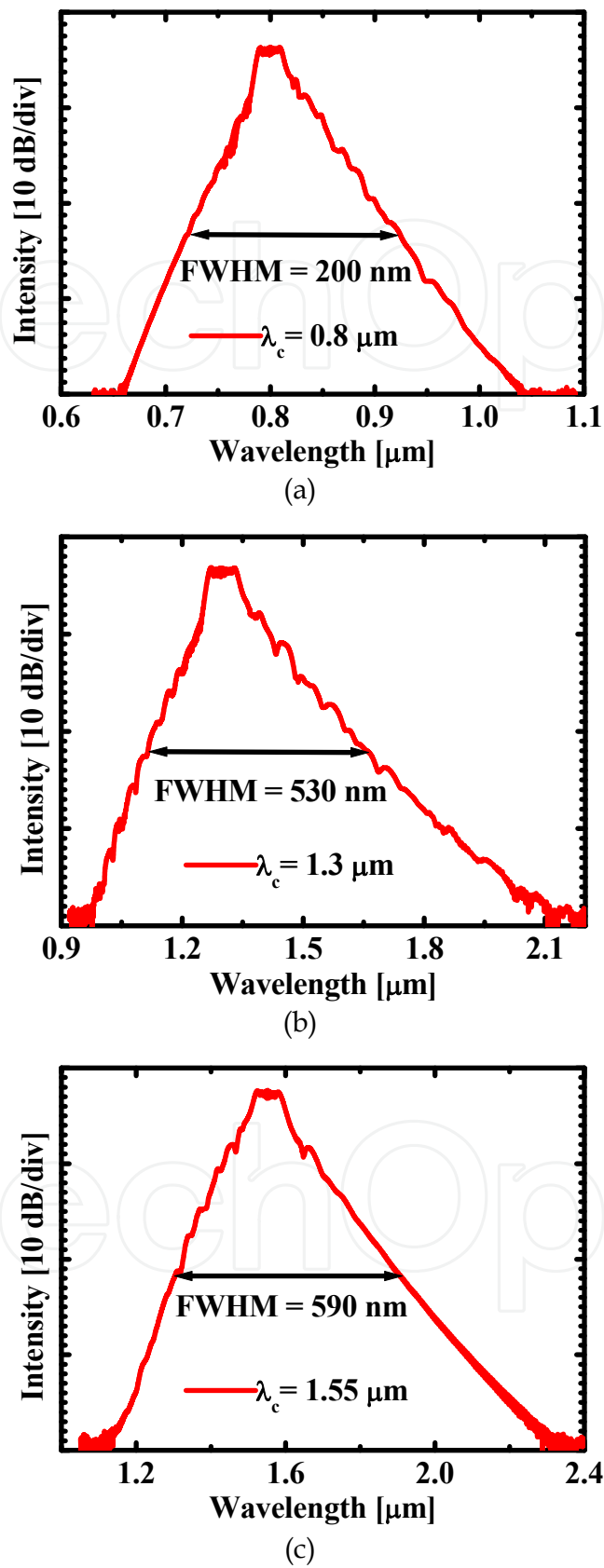
Fig. 4. Spectral intensity at (a) 0.8 µm (b) 1.3 µm and (c) at 1.55 µm of the proposed HN-PCF which is shown in Fig. 1.
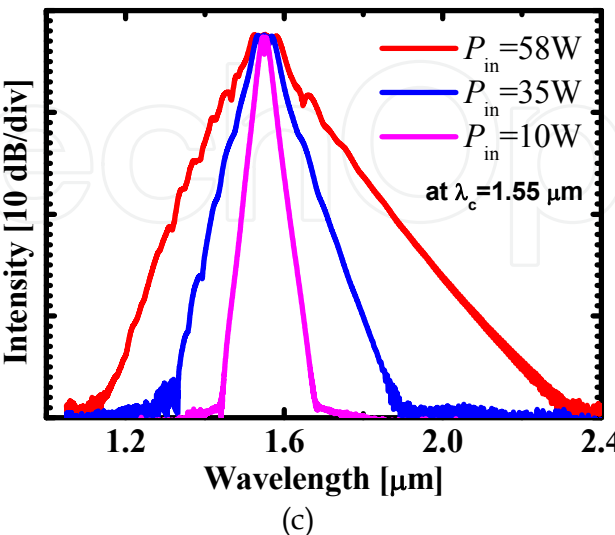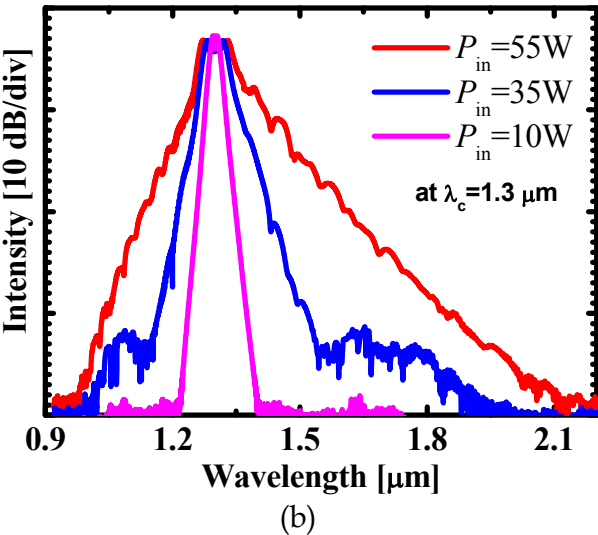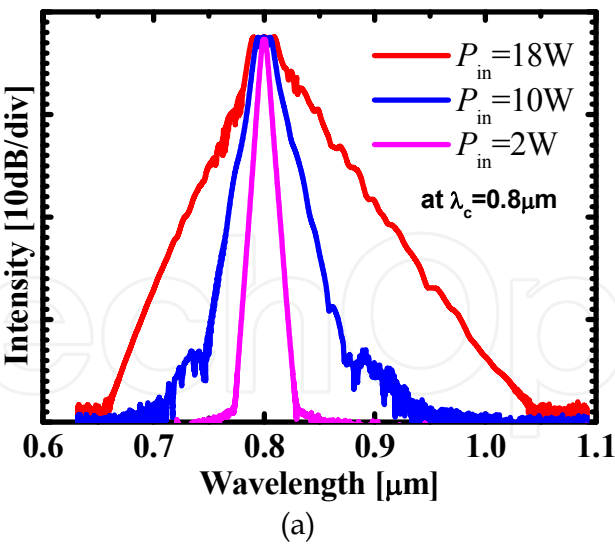
Fig. 5. Intensity spectra at center wavelengths (a) 0.8 µm, (b) 1.3 µm and (c) 1.55 µm of the proposed HN-PCF which is shown in Fig. 1 when changing incident optical powers.
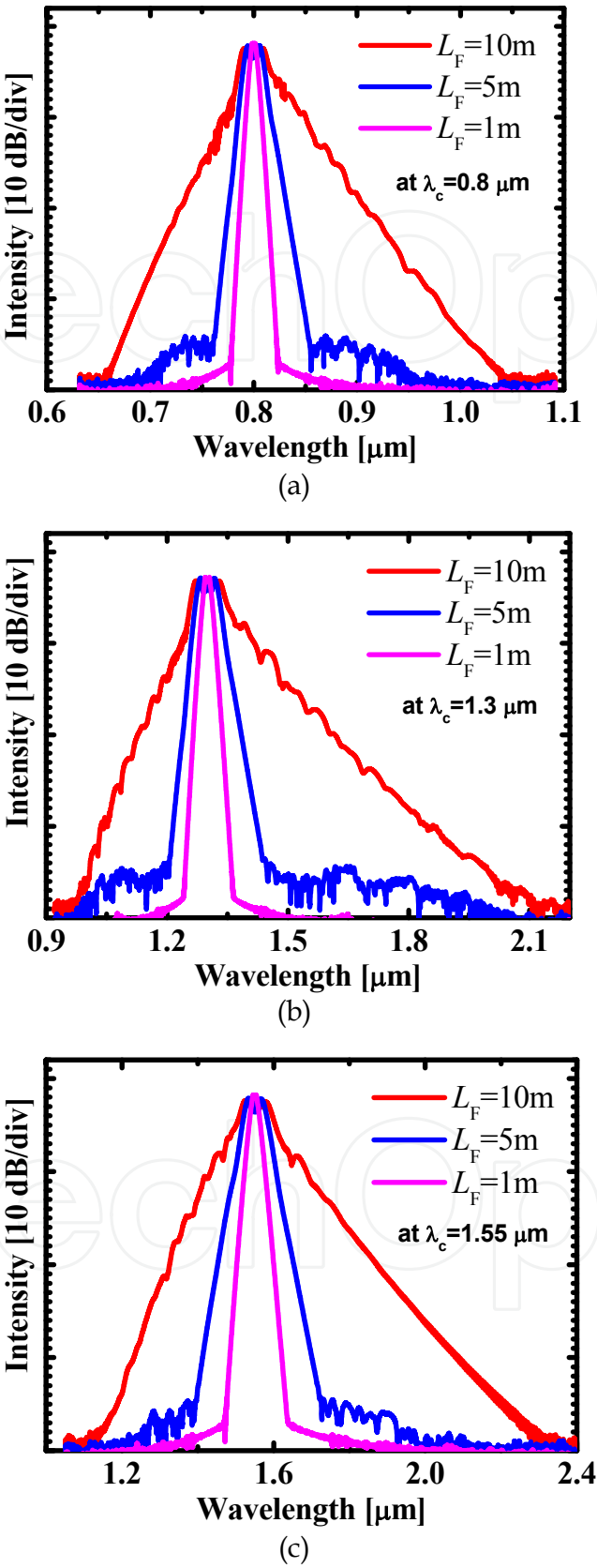
Fig. 6. Intensity spectra at center wavelengths (a) 0.8 µm, (b) 1.3 µm and (c) 1.55 µm of the proposed HN-PCF which is shown in Fig. 1 in different fiber lengths.
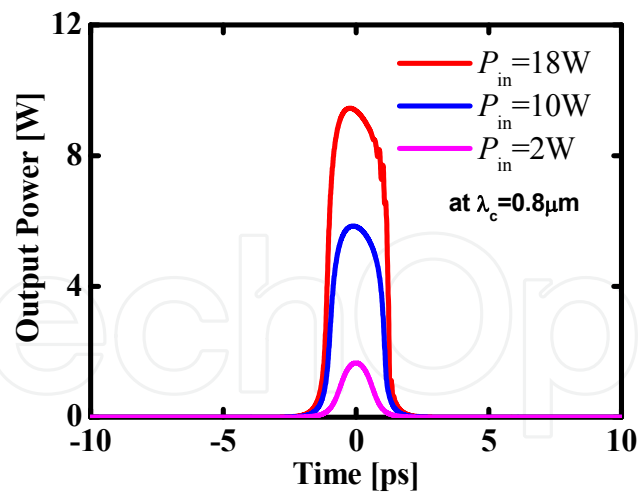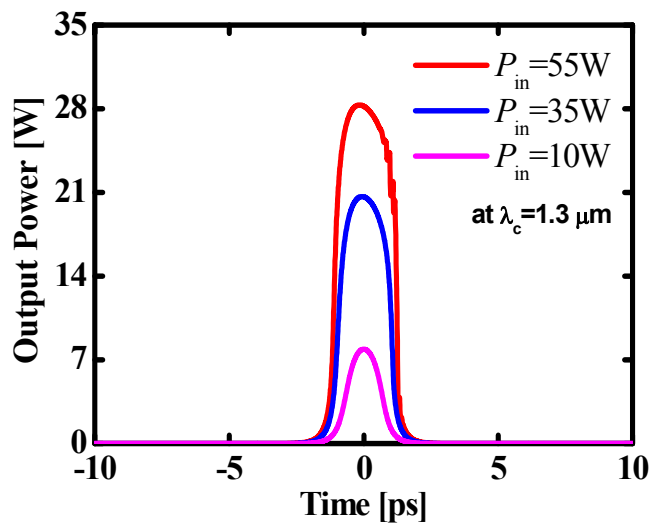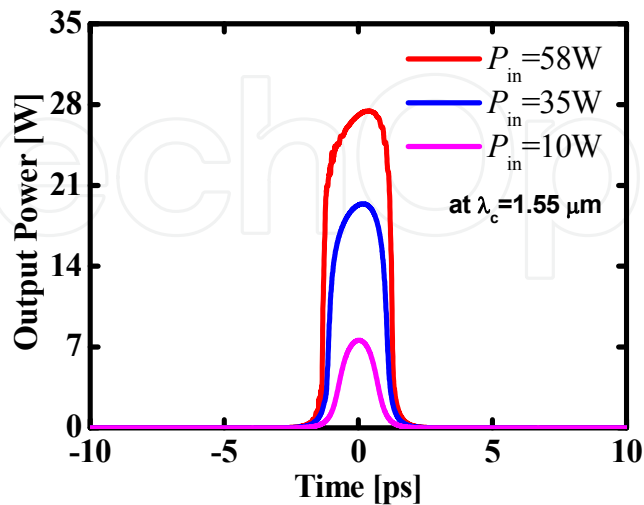
Fig. 7. Output power at center wavelengths (a) 0.8 µm, (b) 1.3 µm and (c) 1.55 µm of the proposed HN-PCF which is shown in Fig. 1.

The spectral bandwidths, FWHM are 200 nm, 530 nm and 590 nm at center wavelength 0.8 µm, 1.3 µm and 1.55 µm, respectively. The calculated l_c values are 1.4 µm, 1.4 µm and 1.8 µm at center wavelength 0.8 µm, 1.3 µm and 1.55 µm, respectively. The calculated l_r values are 0.97 µm, 0.85 µm and 1.1 µm when typical n_{tissue} is 1.44, 1.65 and 1.65 at center wavelengths 0.8 µm, 1.3 µm and 1.55 µm, respectively [Ohmi et al., 2000]. These calculated l_r value is better than that of Ref. [Boppart et al., 1998; Bouma et al., 1995; Colston et al., 1998; Drexler et al., 1999; Hartl et al., 2001; Herz et al., 2004; Jiang et al., 2005; Lee et al., 2009; Ohmi et al., 2004; Pan et al., 1998; Ryu et al., 2005; Tearnery et al., 1997; Welzel et al., 1997] and SLDs with OCT imaging longitudinal resolution of ≈ 10 – 15 µm. Some calculated parameters of the proposed HN-PCF are shown in table 1. From this Table 1, it is seen that the highest longitudinal resolution and wider FWHM is obtained at 1.3 µm and 1.55 µm wavelengths, respectively.

Paramters	λ_c = 0.8 µm	λ_c = 1.3 µm	λ_c = 1.55 µm
β_2 [ps²/km]	1.88	2.55	1.51
β_3 [ps³/km]	0.02	-0.03	0.01
T_R [fs]	3.0	3.0	3.0
T_{FWHM} [ps]	1.0	1.0	1.0
P_{in} [W]	18.0	55.0	58.0
L_F [m]	10.0	10.0	10.0
FWHM [nm]	200.0	530.0	590.0
l_c [µm]	1.4	1.4	1.8
l_r [µm]	0.97	0.85	1.1

Table 1. Some calculated parameters of the proposed HN-PCF.

The apparent advantages of our HN-PCF design are the facts that it simultaneously exhibits numerous optical properties such as flattened dispersion, low confinement loss, high nonlinearity at three central wavelengths 0.8 µm, 1.3 µm and 1.55 µm. Moreover, one can take advantage of the different dispersion characteristics of the two different geometrical parameters to get one more degree of freedom for tailoring the generated SC spectrum. Furthermore, the proposed fiber can be used to make a fiber-based light source to generate SC in three different central wavelengths for ophthalmology, dermatology and dentistry OCT imaging application. Hence, the same fiber with three center wavelengths can be used in several OCT imaging and optical communication applications while exhibiting relatively good longitudinal resolution performance, high power, and in turn can pave the way for the compact, robust and cheap fiber-based OCT light sources. Therefore, picosecond pulse based PCFs are among the most specialized optical lightguides in the new optical fiber technology which is highly competitive compared to traditional laser designs.

5. Conclusions

We have proposed broadband SC generated HN-PCF which can be used as a high power picoseconds pulses light source in ultrahigh-resolution OCT system for ophthalmology, dermatology and dental imaging. Moreover, it has been sent that this proposed HN-PCF would be applicable in optical communication. We achieved longitudinal resolutions in tissue are 0.97 µm, 0.85 µm and 1.1 µm at center wavelength of 0.8 µm, 1.3 µm and 1.55 µm,

respectively. Furthermore, from numerical simulation results it was found that the proposed HN-PCFs have high nonlinear coefficients with ultra-flattened chromatic dispersion, low dispersion slopes, and very low confinement losses, simultaneously. The broad bandwidth of the light source permits high resolution for bright OCT imaging in the wavelength ranges from 0.8 μm to 1.6 μm. For the less number of geometrical parameters, this light source has the potential to be made compact, robust and cheap fiber-based OCT light sources and suitable for clinical applications. Consequently, the same proposed fiber can be used in different optical communication applications such as dispersion controlling, wavelength conversion, SC generation, optical parametric amplification, and so on.

6. Acknowledgement

7. References

Agrawal G.P. (1995). *Nonlinear Fiber Optics*, Academic Press, ISBN 0-12-045142-5

Begum F., Namihira Y., Razzak S.M.A., and Zou N. (2007a). Novel Square Photonic Crystal Fibers with Ultra-flattened Chromatic Dispersion and Low Confinement Losses. *IEICE Trans. on Elec.*, Vol. E90-C, No. 3, pp. 607-612, ISSN 0916-8524

Begum F., Namihira Y., Razzak S.M.A., Kaijage S., Miyagi K., Hai N.H., and Zou N. (2007b). Highly Nonlinear Dispersion-Flattened Square Photonic Crystal Fibers with Low Confinement Losses. *Opt. Review*, Vol. 14, No. 3, pp. 120-124, ISSN 1340-6000

Begum F., Namihira Y., Razzak S.M.A., Kaijage S., Hai N.H., Kinjo T., Miyagi K., and Zou N. (2009a). Novel Broadband Dispersion Compensating Photonic Crystal Fibers: Applications in High Speed Transmission Systems. *Jour. of Opt. & Laser Tech.*, Vol. 41, No. 5, pp. 679-686, ISSN 0030-3992

Begum F., Namihira Y., Kaijage S., Razzak S.M.A., Hai N.H., Kinjo T., Miyagi K., and Zou N. (2009b). Design and analysis of novel highly nonlinear hexagonal photonic crystal fibers with ultra-flattened chromatic dispersion. *Opt. Comm.*, Vol. 282, No. 7, pp. 1416-1421, ISSN 0030-4018

Begum F., Namihira Y., Kinjo T., and Kaijage S. (2011). Supercontinuum generation in square photonic crystal fiber with nearly zero ultra-flattened chromatic dispersion and fabrication tolerance analysis. *Opt. Commun.*, Vol. 284, No. 4, pp. 965-970, ISSN 0030-4018

Boppart S.A., Bouma B.E., Pitris C., Southern J.F., Brezinski M.E., and Fujimoto J.G. (1998). In vivo cellular optical coherence tomography imaging. *Nature Medicine*, Vol. 4, No. 7, pp. 861-865, ISSN 1078-8956

Bouma B.; Tearney G.J.; Boppart S.A.; Hee M.R.; Brezinski M.E., and Fujimoto J.G. (1995). High-resolution optical coherence tomographic imaging using a mode-locked Ti:Al2O3 laser source. *Opt. Lett.*, Vol. 20, No. 13, pp. 1486-1488, ISSN 0146-9592

Colston B.W., Jr., Sathyam U.S., DaSilva L.B., Everett M.J., Stroeve P., and Otis L.L. (1998). Dental OCT. *Opt. Express*, Vol. 3, No. 6, pp. 230-238, ISSN 1094-4087

Couny F., Roberts P.J., Birks T.A., and Benabid F. (2008). Square-lattice large-pitch hollow-core photonic crystal fiber. *Optics Express*, Vol. 16, No. 25, pp. 20626-20636, ISSN 1094-4087

Drexler W., Morgner U., Kärtner F.X., Pitris C., Boppart S.A., Li X.D., Ippen E.P., and Fujimoto J.G. (1999). In vivo ultrahigh-resolution optical coherence tomography. *Opt. Lett.*, Vol. 24, No. 17, pp. 1221-1223, ISSN 0146-9592

Hartl I., Li X.D., Chudoba C., Ghanta R.K., Ko T.H., Fujimoto J.G., Ranka J.K., and Windeler R.S. (2001). Ultrahigh-resolution optical coherence tomography using continuum generation in an air-silica microstructure optical fiber. *Opt. Lett.*, Vol. 26, No. 9, pp. 608-610, ISSN 0146-9592

Herz P.R., Chen Y., Aguirre A.D., Fujimoto J.G., Mashimo H., Schmitt J., Koski A., Goodnow J., and Peterson C. (2004). Ultrahigh resolution optical biopsy with endoscopic optical coherence tomography. *Optics Express*, Vol. 12, No. 15, pp. 3532-3542, ISSN 1094-4087

Jiang Y., Tomov I.V., Wang Y., and Chen Z. (2005). High-resolution second-harmonic optical coherence tomography of collagen in rat-tail tendon. *Applied Physics Lett.*, Vol. 86, No. 13, pp. 133901-133903, ISSN 0003-6951

Kaijage S.F., Namihira Y., Hai N.H., Begum F., Razzak S.M.A., Kinjo T., Higa H., and Zou N. (2008). Multiple Defect-core Hexagonal Photonic Crystal Fiber with Flattened Dispersion and Polarization Maintaining Properties. *Opt. Review,* Vol. 15, No. 1, pp. 31-37, ISSN 1340-6000

Knight J.C., Birks T.A., Russell P.St.J., and Atkin D.M. (1996). All-silica single-mode optical fiber with photonic crystal cladding. *Opt. Lett.*, Vol. 21, No. 19, pp. 1547-1549, ISSN 0146-9592

Knight J.C., Birks T.A., Cregan R.F., Russell P.St.J., and de Sandro J.-P. (1998). Large mode area photonic crystal fiber. *Electron. Lett.*, Vol. 34, No. 13, pp. 1347-1348, ISSN 0013-5194

Lee J.H., Jung E.J., and Kim C.-S. (2009). Incoherent, CW supercontinuum source based on erbium fiber ASE for optical coherence tomography imaging. *Proceedings of OptoEelectronics and Communication Conference*, Paper number FD3, Hongkong, 13-17 July 2009, ISBN 978-1-4244-4102-0

Ohmi M., Ohnishi Y., Yoden K., and Haruna M. (2000). In vitro simultaneous measurement of refractive index and thickness of biological tissue by the low coherence interferometry. *IEEE Trans. on Biomed. Eng.*, Vol. 47, No. 9, pp. 1266-1270, ISSN 0018-9294

Ohmi M., Yamazaki R., Kunizawa N., Takahashi M., and Haruna M. (2004). In vivo observation of micro-tissue structures by high-resolution optical coherence tomography with a femtosecond laser. *Japanese Society for Medical and Biological Engineering (Japanese paper)*, Vol. 42, No. 4, pp. 204-210, ISSN 1881-4379

Pan Y., and Farkas DL. (1998). Noninvasive imaging of living human skin with dual-wavelength optical coherence tomography in two and three dimensions. *J Biomed Opt.*, Vol. 3, No. 4, pp. 446–455, ISSN 1083-3668

Russel P.St.J. (2003). Photonic crystal fibers. *Science*, Vol. 299, No. 5605, pp. 358-362, ISSN 0036-8075

Ryu S.Y., Choi H.Y., Choi J.N.E., Yang G.-H. and Lee B.H. (2005). Optical Coherence tomography implemented by photonic crystal fiber. *Opt. and Quantum Elec.*, Vol. 37, No. 13-15, pp. 1191-1198, ISSN 0306-8919

Shen L.-P., Huang W.-P., and Jian S.-S. (2003). Design of photonic crystal fibers for dispersion-related applications. *J. Lightwave Technol.*, Vol. 21, No. 7, pp. 1644-1651, ISSN 0733-8724

Tearney G.J., Bouma B.E., and Fujimoto J.G. (1997). High-speed phase- and group-delay scanning with a grating-based phase control delay line. *Opt Lett.*, Vol. 22, No. 23, pp. 1181–1183, ISSN 0146-9592

Welzel J., Lankenau E., Birngruber R., and Engelhardt R. (1997). Optical coherence tomography of the human skin. *J Am Acad Dermatol.*, Vol. *37*, No. 6, pp. 958–963, ISSN 0190-9622
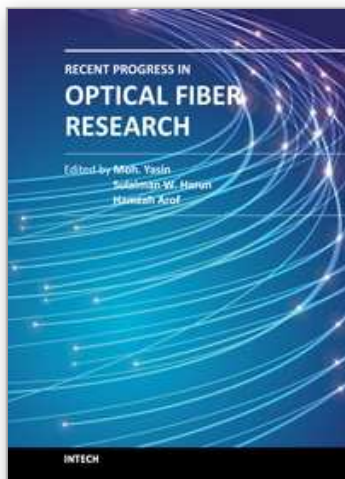
Recent Progress in Optical Fiber Research
Edited by Dr Moh. Yasin

This book presents a comprehensive account of the recent progress in optical fiber research. It consists of four sections with 20 chapters covering the topics of nonlinear and polarisation effects in optical fibers, photonic crystal fibers and new applications for optical fibers. Section 1 reviews nonlinear effects in optical fibers in terms of theoretical analysis, experiments and applications. Section 2 presents polarization mode dispersion, chromatic dispersion and polarization dependent losses in optical fibers, fiber birefringence effects and spun fibers. Section 3 and 4 cover the topics of photonic crystal fibers and a new trend of optical fiber applications. Edited by three scientists with wide knowledge and experience in the field of fiber optics and photonics, the book brings together leading academics and practitioners in a comprehensive and incisive treatment of the subject. This is an essential point of reference for researchers working and teaching in optical fiber technologies, and for industrial users who need to be aware of current developments in optical fiber research areas.

How to reference

In order to correctly reference this scholarly work, feel free to copy and paste the following:

Feroza Begum and Yoshinori Namihira (2012). Photonic Crystal Fiber for Medical Applications, Recent Progress in Optical Fiber Research, Dr Moh. Yasin (Ed.), ISBN: 978-953-307-823-6, InTech, Available from: http://www.intechopen.com/books/recent-progress-in-optical-fiber-research/photonic-crystal-fiber-for-medical-applications-

INTECH
open science | open minds